SCIENTIFIC REPORTS

OPEN

First-principles study of nonmetal doped monolayer MoSe$_2$ for tunable electronic and photocatalytic properties

Yafei Zhao[1], Wei Wang[1], Can Li[2] & Liang He[1]

Recently, two dimensional transition metal dichalcogenides become popular research topics because of their unique crystal and electronic structure. In this work, the geometrical structure, electronic, electrical transport, redox potentials and photocatalytic properties of nonmetal (H, B, C, Si, N, P, As, O, S, Te, F, Cl, Br and I) doped monolayer MoSe$_2$ were investigated by first principle calculations. The binding energy indicates that nonmetal doped MoSe$_2$ are energetically favorable compared to Se vacancies, except B- and C-doped. We have found that nonmetal dopants with an even number of valence electrons doped MoSe$_2$ have p-type conductivity. On the contrary, nonmetal dopants with an odd number of valence electrons doped MoSe$_2$ have p-type or n-type conductivity; and they have better photocatalytic performance.

Transition metal dichalcogenides (TMDCs) have unique structural and electronic properties. Consequently, they possess various conducting properties that include insulating, semiconducting, conducting and even super-conducting. And these cause potential applications in electronics, spintronics and optoelectronics[1–8]. TMDCs family has more than 40 compounds (including MoS$_2$, WS$_2$, MoSe$_2$, WSe$_2$ and WTe$_2$ *etc*) with the formula of MX$_2$[9,10]. These TMDCs materials have been obtained by micromechanical exfoliation or liquid exfoliation (due to the weak van der Waals bonding interactions in the adjacent sandwiched layers)[11–13], chemical vapor deposition (CVD)[14] and molecular beam epitaxy (MBE)[15,16]. However, vacancies inevitably occur in the growth process of TMDCs[17–19].

The introduction of dopant atoms into the vacancies is considered as a promising method of modulating their electronic, magnetic and transport properties of monolayer TMDCs[20–29]. Experimentally, Zn- and Co-doped MoS$_2$ nanosheets have been realized and demonstrate potential applications in the field of electronics, opto-electronics, spintronics and photocatalysis[30,31]. Moreover, a series of work have reported that ultrathin N- and P-doped MoS$_2$ nanosheets have demonstrated enhanced hydrogen evolution reaction (HER) catalysis, enhanced oxygen reduction reaction (ORR) and efficient degradation of methyl orange and RhB, respectively[32–36]. This is due to they can promote the charge transfer in the photocatalytic reaction. These results suggest that doping non-metal (NM) atoms is an effective way to promote the catalytic performance.

However, the above articles lack the calculations on the electrical transport of NM doped systems. Moreover, systematically understanding the modification on the physical and chemical properties of the NM doped monolayer MoSe$_2$ is necessary. In this work, we provide a comprehensive investigation on the geometrical structure, binding energy, electronic, optical and photocatalytic properties of substitutionally doped monolayer MoSe$_2$ with a series of NM atoms, such as H, B, C, Si, N, P, As, O, S, Te, F, Cl, Br and I, by employing first-principle calculations. And we found the parity of the valence electrons of the dopants causes a dramatic difference on electrical transport, molecular state, redox potentials and photocatalytic activity.

Computational Methods

The geometrical structure, electronic and optical properties of undoped and NM doped monolayer MoSe$_2$ are calculated within the framework of density functional theory by using the CASTEP package. Norm-conserving

[1]National Laboratory of Solid State Microstructures, School of Electronic Science and Engineering and Collaborative Innovation Center of Advanced Microstructures, Nanjing University, Nanjing, 210093, China. [2]Center for Coordination Bond Engineering, College of Materials Science and Engineering, China Jiliang University, Hangzhou, 310018, China. Correspondence and requests for materials should be addressed to L.H. (email: heliang@nju.edu.cn)
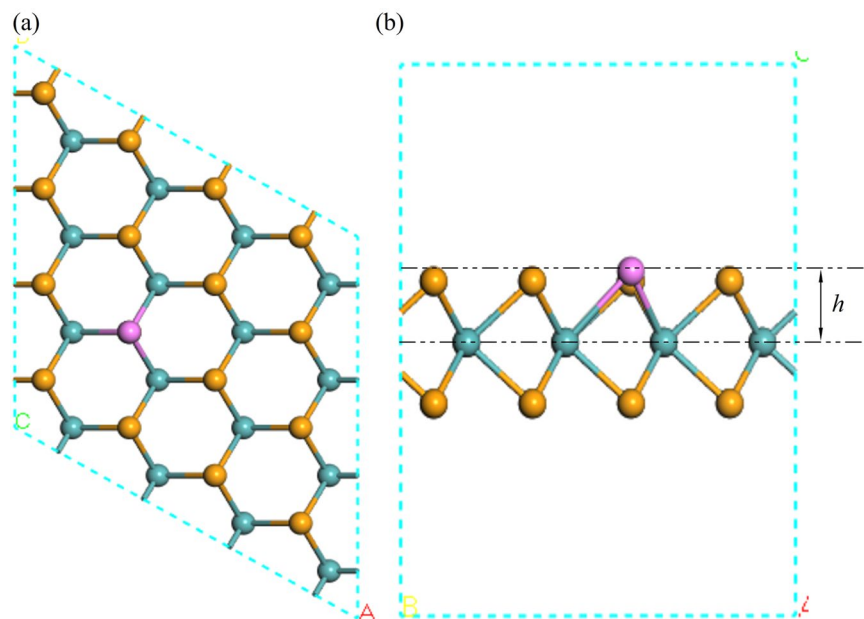
Figure 1. (**a**) Top view and (**b**) side view of the crystal structure of a $4 \times 4 \times 1$ doped supercell monolayer MoSe$_2$. The blue, yellow and purple spheres denote the Mo, Se and NM atoms, respectively.

Dopant	a	$d_{\text{Mo-NM}}$	h	E_b	E_F	E_{VBM}	E_{CBM}	E_g
H	3.332	2.054	0.888	0.13	−3.00	−3.95	−2.29	1.66
B	3.350	2.145	0.801	−0.85	−3.75	−4.00	−2.35	1.65
C	3.344	2.041	0.795	−0.81	−3.38	−3.38	−1.82	1.56
Si	3.364	2.415	1.181	0.13	−3.30	−3.30	−1.84	1.46
N	3.337	2.018	0.927	0.46	−3.54	−3.91	−2.35	1.56
P	3.348	2.446	1.531	1.19	−3.80	−3.80	−2.26	1.54
As	3.349	2.595	1.749	0.92	−3.86	−3.86	−2.30	1.56
O	3.332	2.088	1.047	3.78	−3.40	−3.40	−1.81	1.63
S	3.346	2.436	1.522	2.67	−3.39	−3.39	−1.76	1.61
undoped	3.351	2.570	1.641	—	−3.36	−3.36	−1.74	1.62
Te	3.358	2.762	1.932	2.04	−3.33	−3.33	−1.73	1.60
F	3.341	2.276	1.253	0.34	−2.52	−3.94	−2.28	1.66
Cl	3.353	2.534	1.621	1.31	−2.43	−3.92	−2.43	1.51
Br	3.358	2.673	1.803	1.04	−2.45	−3.90	−2.27	1.63
I	3.363	2.853	2.037	0.94	−2.48	−3.87	−2.26	1.61

Table 1. The equilibrium supercell lattice parameters a with unit Å. $d_{\text{Mo-NM}}$ is the bond lengths of Mo-NM bonds with unit Å. h is the sheet thicknesses from NM atom to the reference Mo atom plane with unit Å. E_b, E_g E_F, E_{CBM} and E_{VBM} are the calculated binding energies, band gap, Fermi level, the energy edge of CBM and VBM relative to vacuum level, respectively, with unit eV.

pseudopotentials and Perdew-Burke-Ernzerhof (PBE) function of the generalized gradient approximation (GGA) are used for the electron-ion interactions and exchange-correlation potential, respectively[37,38]. The adopted monolayer structure is a $4 \times 4 \times 1$ supercell containing 16 Mo (blue ball), 31 Se (yellow ball) and 1 NM atoms (purple ball) (Fig. 1(a)). The high cutoff energy for the plane-wave basis is set at 750 eV and the Brillouin zone is sampled by a $9 \times 9 \times 1$ k-point sampling grid. A vacuum layer of 15 Å is adopted in the direction perpendicular to the monolayer surface to avoid the interactions between periodic slabs. The structural optimization is continued until the convergence tolerance of energy, maximum force and maximum displacement are less than 5.0×10^{-6} eV/atom, 0.01 eV/Å and 1.0×10^{-3} Å, respectively.

We have calculated the binding energies (E_b) of all the doped systems to assess the stability of doped MoSe$_2$:

$$E_b = E_{\text{vacany}} + \mu_{\text{NM}} - E_{\text{doped}} \tag{1}$$
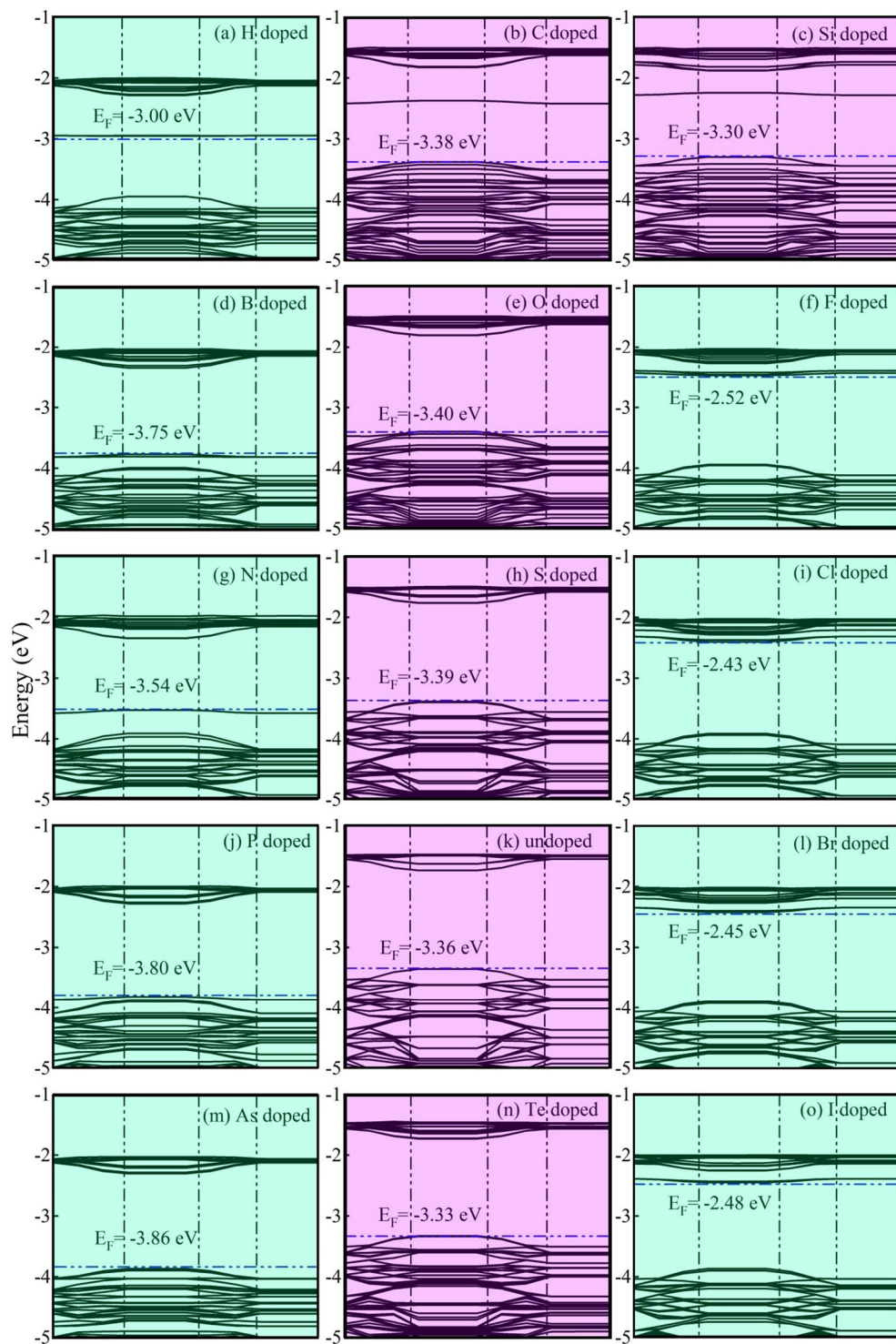
Figure 2. The band structures of undoped and NM doped monolayer MoSe$_2$. The light blue and light purple background colors are represent the band structures of the odd and even number valence electrons doped systems, respectively. NM dopants with an even number of valence electrons are generally p-type conductivity. On the contrary, NM dopants with an odd number of valence electrons can provide effective p-type or n-type conductivity.

where E_{doped} is the total energy of the monolayer MoSe$_2$ with one Se atom replaced by the NM atom, E_{vacany} is the total energy of the monolayer MoSe$_2$ with one Se vacancy, and μ_{NM} is the chemical potential of the dopant and is calculated with respect to the elemental bulk or gas in nature. Positive E_b suggests that doped atom is energetically favorable to sit at the substitutional site of Se.
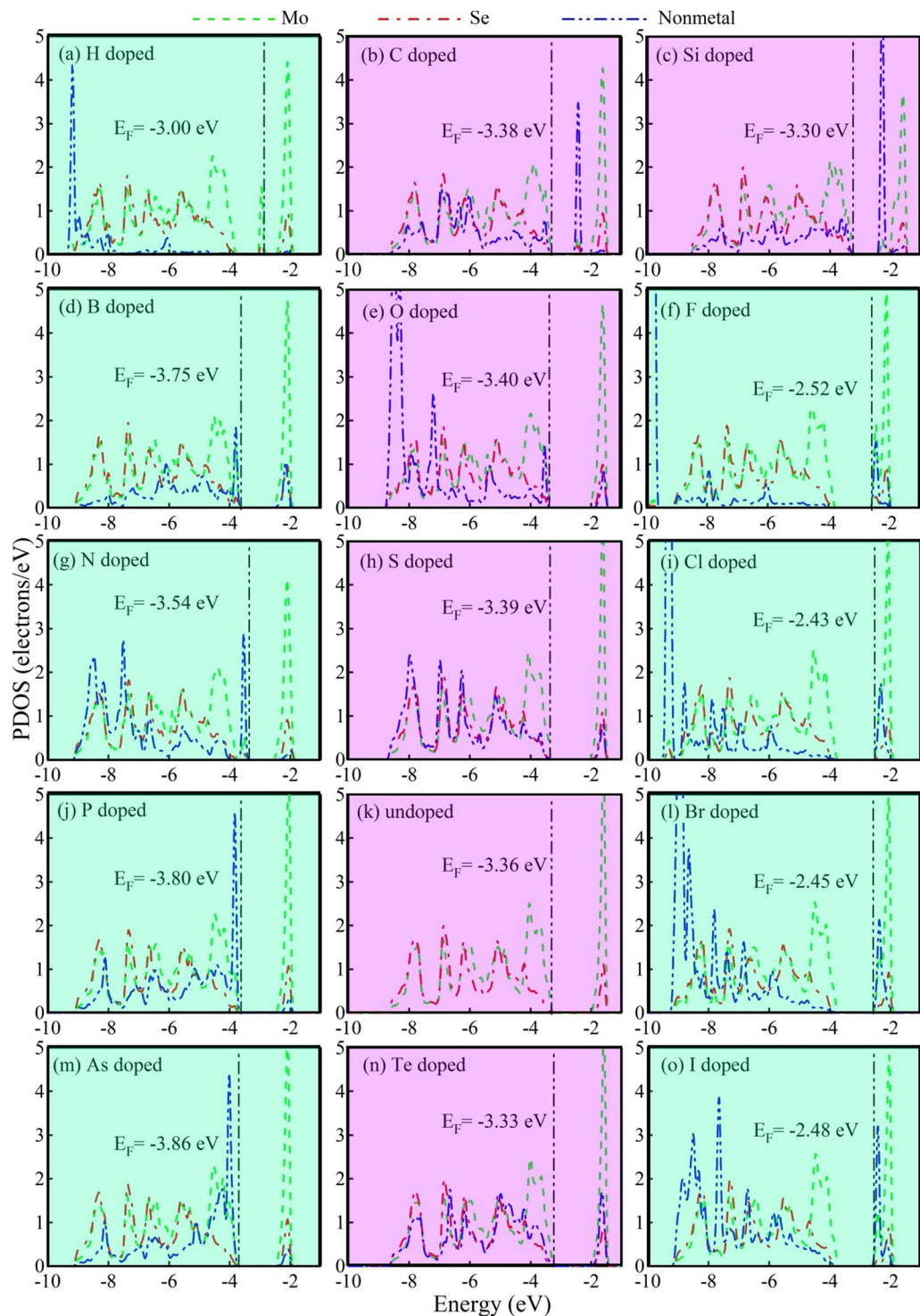
Figure 3. The average PDOS of Mo, Se and NM atoms of undoped and NM doped monolayer MoSe$_2$.

Results and Discussions

Binding energies and optimized Structures. Table 1 lists the calculated results of the doped systems. All of them (except for B- and C-doped) have positive E_b, indicating that their formations are exothermic reaction and therefore stable. The E_b of the VIA (O, S and Te) group doped is the largest (>2 eV). This is due to the dopants have the same valence electron structure as Se. Thus they are most stable when fill up the Se vacancy. O-doped system, overall, has the largest E_b (3.78 eV), since O atom has the highest electronegativity. The E_b of the VA (N, P and As) and VIIA (F, Cl, Br and I) group doped are smaller (~1 eV). This is probably due to the absent or extra one electron cost some formation energy. Doping of NM atoms with the IA (H), IIIA (B) and IVA (C and Si) groups is less energetically favorable, with E_b of ~0 eV. This can be attributed to their valence electron structures have the largest difference compared with Se.
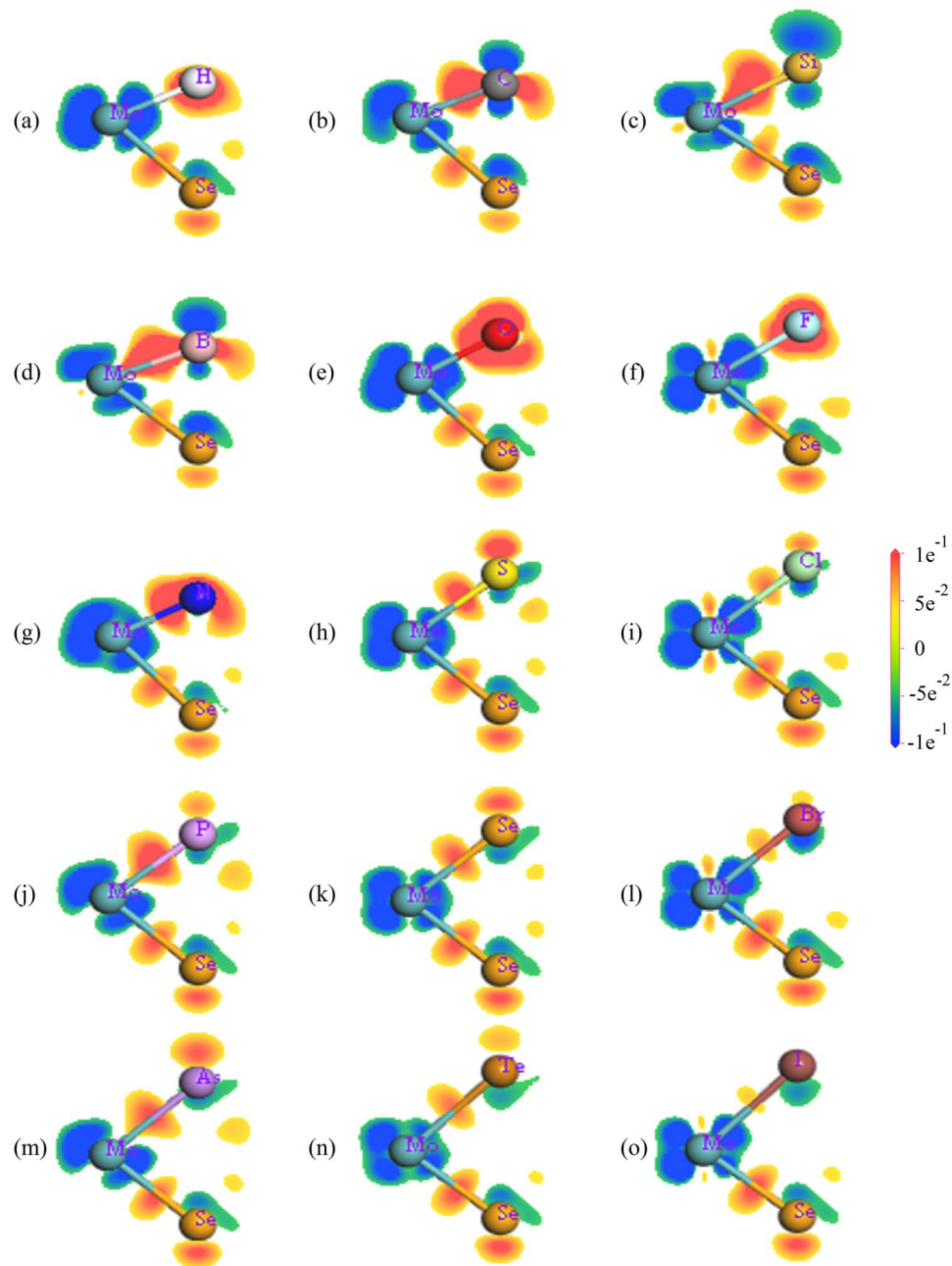
Figure 4. The electron density difference of undoped and NM doped monolayer $MoSe_2$. Mo-4d and Se-4p states (green and red lines) are basically invariable, while the NM-p (or -s) states (blue lines) demonstrate huge difference. Thus, the dopants can only affect the local electronic structure.

Although their E_b varies a lot, their lattice structures stay constant, within 0.6%. On the other hand, the local structure and the electronic properties have been modified dramatically. The Mo-NM bond lengths (d_{Mo-NM}) and h (the sheet thicknesses from NM atom to the reference Mo atom plane, Fig. 1(b)) of doped $MoSe_2$ vary as much as 21.5% and 51.6%, respectively. This is mostly due to the variation of the atomic radius and electronegativity of NM atoms. More details will be discussed later.

Electronic and electrical transport properties. To explain how doped NM atoms modify the electronic properties of monolayer $MoSe_2$, we have calculated the band structures and partial density of states (PDOS) of individual Mo, Se and NM atoms of all the systems, as shown in Figs 2 and 3, respectively. For undoped monolayer $MoSe_2$, conduction band (CB) and valence band (VB) are composed of Mo-4d and Se-4p states, and each Mo atom can provide four electrons interacting with the surrounding six Se atoms. For IVA (C and Si) and VIA (O, S and Te) group doped systems (NM dopants with even number of valence electrons), the Fermi level (E_F) of doped $MoSe_2$ is almost unchanged ($-0.04 \sim 0.06$ eV, see Table 1) compared to the undoped one and is slightly above the valence band maximum (VBM), seen in Fig. 2. These phenomena are consistent with the results in C-,
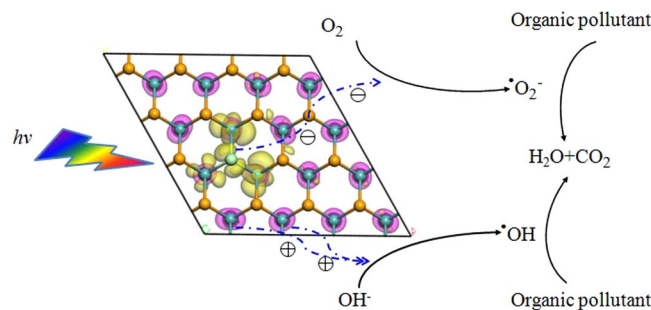
Figure 5. The mechanism of photocatalytic degrading organic pollutant and the charge dynamics in VIIA doped monolayer $MoSe_2$. The purple and yellow regions represent HOMO and LUMO, respectively. Under light irradiation, the photogenerated e^- moves to Mo atoms and VIIA group atoms in the yellow region, while, photogenerated h^+ moves only on the Mo atoms in the purple region. This represents the separation of photogenerated e^-/h^+ in real space.
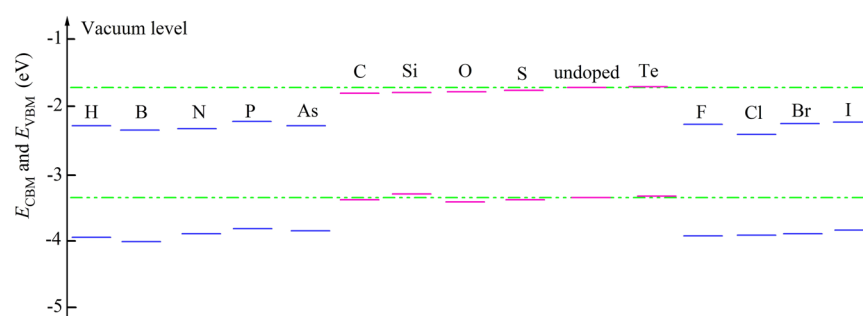

Figure 6. The E_{CBM} and E_{VBM} of undoped (green dotted line) and NM doped monolayer $MoSe_2$. Dopants with odd number of valence electrons doped $MoSe_2$ have lower E_{VBM}, suggesting the oxidation of their photogenerated holes is enhanced compared with undoped $MoSe_2$.

Si-, O-, Se- and Te-doped monolayer MoS_2 or WSe_2[21,28,29]. Thus, NM dopants with an even number of valence electrons doped monolayer $MoSe_2$ is still generally a p-type semiconductor.

For IIIA (B) and VA (N, P and As) group doped cases, the E_F lowered about 0.18~0.50 eV compared to the undoped one. The similar results have also been reported in B- N-, P- and As-doped monolayer MoS_2 or WSe_2 and N-, P- and As-doped monolayer $MoSe_2$[21,28,39,40]. Thus, they are still a p-type semiconductor. For IA (H) group doped case, a half-filled impurity level (mostly composed of Mo-$4d$ states) appears within the band gap and lifts the E_F into the middle of the band gap. Thus p-type conductivity is suppressed. For VIIA (F, Cl, Br and I) group doped systems, an additional valence electron results in the donor impurity level (consisting Mo-$4d$ and NM-p states) and the E_F is lifted close to the conduction band minimum (CBM). Thus, they become an n-type semiconductor, consistent with the reported results[21,28,39,40]. Thus, we can conclude that NM dopants with an odd number of valence electrons doped $MoSe_2$ can have p-type or n-type conductivity. On the contrary, NM dopants with an even number of valence electrons can only provide p-type conductivity. This suggests a possible way to realize bipolar electrical transport properties by tuning the dopants, which is essential for practical applications in optoelectronics and electronics.

We further observe the PDOS of all doped systems found that Mo-$4d$ (green lines) and Se-$4p$ states (red lines) are basically invariable, while the NM-p (or -s) states (blue lines) demonstrate huge difference (see Fig. 3). Therefore, we believe that the dopants can only affect the local electronic structure. This is also verified by the calculated electronic density difference. Overall, the dopants only affect the electronic distribution of the three nearest neighboring Mo atoms, other atoms are unaffected. Thus, in Fig. 4, we only demonstrate the electronic density difference of the NM and the closest Mo and Se atoms. The blue (or red) regions indicate the electron loss (or accumulation), and the red regions between the two atoms indicate that they form a covalent bond. Thus, the Se and the Mo atom are ionized; meanwhile, a covalent bond is formed between them in undoped monolayer $MoSe_2$. It is found that Mo-NM ionic bonds are formed in the N-, O- and F-doped system, due to their large electronegativity. On the other hand, covalent bonds with different strength are formed for other dopants. Thus we believe the change of the globe electronic properties of the doped $MoSe_2$ is due to this local change of electron distribution.

Optical and photocatalytic properties. We have also calculated the optical properties of all the systems and the results show that NM dopants slightly affect the optical absorption edge and optical absorption areas in the range of 300 to 900 nm (see Supplementary Fig. S1). On the other hand, this work also provides the

highest occupied molecular state (HOMO) and lowest unoccupied molecular state (LOMO) of all the systems (show in Fig. S2). We have found that the physical location of HOMO and LUMO can be tuned by different NM dopants[28,41].

For undoped $MoSe_2$, the HOMO and LUMO are made up of Mo-4d states, thus they are located at all the Mo atoms simultaneously (Fig. S2(k)). And the photogenerated electrons (e^-) and holes (h^+) will be easily recombined on Mo atoms, which reduce the photocatalytic efficiency. For IVA (C and Si) group doped $MoSe_2$, both the HOMO and LUMO mainly locate at the NM atom and its three nearest Mo atoms. For VIA (O, S and Te) group doped $MoSe_2$, similar to undoped $MoSe_2$, both the HOMO and LUMO mainly locate at the Mo atoms across the film. Thus, in these two cases, the photogenerated electrons e^-/h^+ have a good chance to recombine.

For IA (H) group and VIIA (F, Cl, Br and I) group doped $MoSe_2$, the distribution of HOMO states is the same as the undoped $MoSe_2$, while the LUMO states are mainly located at the NM atom and its three nearest Mo atoms. For IIIA (B) doped $MoSe_2$, the distribution is opposite to them. For VA (N, P and As) group doped $MoSe_2$, the HOMO states locate at around NM atom and its surrounding Mo atoms, and the LUMO states locate at Mo atoms further away from NM atoms. In these three cases, the HOMO and LUMO states are separated in real space.

O_2^- ion and OH radical are important oxidants for the degradation of organic pollutants. As an example, the schematic mechanism of photocatalytic degrading process is shown in Fig. 5 for VIIA (F, Cl, Br and I) group doped $MoSe_2$ system. Under light irradiation, the e^- and h^+ will be generated at the yellow and purple region, respectively. Next, O_2^- ions and ·OH radicals can be reduced or oxidized by the e^- or h^+, simultaneously. And they can oxidize the organic pollutant into H_2O and CO_2. Thus, due to the separation of the HOMO and LUMO states in the real space, NM dopants with an odd number of valence electrons doped monolayer $MoSe_2$ can suppress the recombination probability of the photogenerated e^- and h^+, and increase the photocatalytic performance.

Further, the VBM and CBM position are calculated relative to vacuum level[42,43], see Fig. 6 and Table 1, the oxidation potential of the photogenerated h^+ is enhanced by 0.44~0.64 eV, while the reduction potential of photogenerated e^- is reduces by 0.52~0.69 eV in the NM dopants with odd number of valence electrons (IA, IIIA, VA and VIIA) doped monolayer $MoSe_2$. On the contrary, the NM dopants with even number of valence electrons even (IVA and VIA doped $MoSe_2$ barely changed the redox potential. Thus, NM dopants with odd number of valence electrons can modify the redox potentials, and tends to generate more ·OH radical than O_2^- ion in the photocatalytic reaction. This is consistent with the experimental report that the ·OH radical played a dominant role in the visible light photocatalytic degradation of RhB for the B/C-doped TiO_2[44].

Conclusions

In this work, the geometrical structure, electrical transport, redox potentials, molecular state, optical and photocatalytic properties of NM doped monolayer $MoSe_2$ are studied by first principle calculations. The E_b suggests that NM doped $MoSe_2$ are energetically favorable compared to Se vacancies, except B- and C-doped $MoSe_2$. We have found that NM dopants with odd number of valence electrons doped monolayer $MoSe_2$ can be p-type or n-type, while dopants with even valence electrons doped ones tend to be p-type. This provides a useful method to realize bipolar electrical transport properties by tuning the dopants for the applications in optoelectronics and electronics. We have also found NM dopants with odd number of valence electrons doped $MoSe_2$ have better photocatalytic performance, due to they can suppress the recombination of photogenerated e^- and h^+, and enhance the oxidation potential of the holes.

References

1. Tian, T. *et al*. Multiscale analysis for field-effect penetration through two-dimensional materials. *Nano. Lett.* **16**, 5044–5052 (2016).
2. Zhou, G. D. *et al*. Investigation of the behaviour of electronic resistive switching memory based on $MoSe_2$-doped ultralong Se microwires. *Appl. Phys. Lett.* **109**, 143904 (2016).
3. Kim, Y., Huang, J. L. & Lieber, C. M. Characterization of nanometer scale wear and oxidation of transition metal dichalcogenide lubricants by atomic force microscopy. *Appl. Phys. Lett.* **59**, 3404 (1991).
4. Mak, K. F. *et al*. Atomically thin MoS_2: A new direct-gap semiconductor. *Phys. Rev. Lett.* **105**, 136805 (2010).
5. Mak, K. F. *et al*. Control of valley polarization in monolayer MoS_2 by optical helicity. *Nat. Nano.* **7**, 494–498 (2012).
6. Sanchez, O. L. *et al*. Ultrasensitive photodetectors based on monolayer MoS_2. *Nat. Nano.* **8**, 497–501 (2013).
7. Zhu, Z., Peelaers, H. & Walle, C. G. V. D. Hydrogen intercalation in MoS_2. *Phys. Rev. B* **94**, 085426 (2016).
8. Kadioglu, Y., Gokoglu, G. & Aktürk, O. U. Effects of gold based dimers on structural and electronic properties of MoS_2. *Appl. Surf. Sci.* **396**, 455–460 (2017).
9. Jiang, Q. Q. *et al*. Facile solvent-thermal synthesis of ultrathin $MoSe_2$ nanosheets for hydrogen evolution and organic dyes adsorption. *Appl. Surf. Sci.* **402**, 277–285 (2017).
10. Ma, D. W. *et al*. The adsorption of CO and NO on the MoS_2 monolayer doped with Au, Pt, Pd, or Ni: A first-principles study. *Appl. Surf. Sci.* **383**, 98–105 (2016).
11. Radisavljevic, B., Brivio, J., Giacometti, V. & Kis, A. Single-layer MoS_2 transistors. *Nat. Nanotechnol.* **6**, 147–150 (2011).
12. Coleman, J. N. *et al*. Two-dimensional nanosheets produced by liquid exfoliation of layered materials. *Science* **331**, 568–571 (2011).
13. Ding, Y. *et al*. First principles study of structural, vibrational and electronic properties of graphene-like MX_2 (M = Mo, Nb, W, Ta; X = S, Se, Te) monolayers. *Physica. B* **406**, 2254–2260 (2011).
14. OBrien, M. *et al*. Low wavenumber Raman spectroscopy of highly crystalline $MoSe_2$ grown by chemical vapor deposition. *Phys. Status. Solidi. B* **252**, 2385–2389 (2015).
15. Mo, S. K. *et al*. Spin-resolved photoemission study of epitaxially grown $MoSe_2$ and WSe_2 thin films. *J. Phys.: Condens. Matter.* **28**, 454001 (2016).
16. Zhang, Q. *et al*. Bandgap renormalization and work function tuning in $MoSe_2$/hBN/Ru (0001) heterostructures. *Nat. Commun.* **7**, 13843 (2016).
17. Zhou, W. *et al*. Intrinsic structural defects in monolayer molybdenum disulfide. *Nano. Lett.* **13**, 2615–2622 (2013).
18. Zheng, H. L., Yang, B. S. & Wang, D. D. Tuning magnetism of monolayer MoS_2 by doping vacancy and applying strain. *Appl. Phys. Lett.* **104**, 132403 (2014).
19. Zou, X., Liu, Y. & Yakobson, B. I. Predicting dislocations and grain boundaries in two-dimensional metal-disulfides from the first principles. *Nano. Lett.* **13**, 253–258 (2013).

20. Kong, L. J., Liu, G. H. & Qiang, L. Electronic and optical properties of O-doped monolayer MoS$_2$. *Comp. Mater. Sci.* **111**, 416–423 (2016).
21. Lu, S. *et al.* Tunable redox potential of nonmetal doped monolayer MoS$_2$: First principle calculations. *Appl. Surf. Sci.* **384**, 360–367 (2016).
22. Cheng, Y. C. *et al.* Prediction of two-dimensional diluted magnetic semiconductors: doped monolayer MoS$_2$ systems. *Phys. Rev. B* **87**, 100401 (2013).
23. Suh, J. *et al.* Doping against the native propensity of MoS$_2$: degenerate hole doping by cation substitution. *Nano. Lett.* **14**, 6976–82 (2014).
24. Mishra, R. *et al.* Long-range ferromagnetic ordering in manganese-doped two-dimensional dichalcogenides. *Phys. Rev. B* **88**, 144409 (2013).
25. Yang, Y. *et al.* First-principles investigations of transition-metal doped bilayer WS$_2$. *Phys. Chem. Chem. Phys.* **18**, 10152–10157 (2016).
26. Qi, L., Wang, Y., Shen, L. & Wu, Y. H. Chemisorption-induced n-doping of MoS$_2$ by oxygen. *Appl. Phys. Lett.* **108**, 063103 (2016).
27. Ma, D. W. *et al.* Modulating electronic, magnetic and chemical properties of MoS$_2$ monolayer sheets by substitutional doping with transition metals. *Appl. Surf. Sci.* **364**, 181–189 (2016).
28. Lu, S. *et al.* The effects of nonmetal dopants on the electronic, optical, and catalytic performances of monolayer WSe$_2$ by a first-principles study. *RSC. Adv.* **6**, 114109–114122 (2016).
29. Hu, A. M. *et al.* Electronic structures and magnetic properties in nonmetallic element substituted MoS$_2$ monolayer. *Comp. Mater. Sci.* **107**, 72–78 (2015).
30. Xu, E. Z. *et al.* p-Type transition-metal doping of large-area MoS$_2$ thin films grown by chemical vapor deposition. *Nanoscale* **9**, 3576 (2017).
31. Wang, Y. R., Li, S. A. & Yi, J. B. Electronic and magnetic properties of Co doped MoS$_2$ monolayer. *Sci. Rep.* **6**, 24153 (2016).
32. Liu, P. T. *et al.* Flower-like N-doped MoS$_2$ for photocatalytic degradation of RhB by visible light irradiation. *Nanotechnology* **27**, 225403 (2016).
33. Hao, L. *et al.* Nitrogen-doped MoS$_2$/carbon as highly oxygen-permeable and stable catalysts for oxygen reduction reaction in microbial fuel cells. *J. Power. Sources.* **339**, 68–79 (2017).
34. Zhang, H. Y. *et al.* Small dopants make big differences: enhanced electrocatalytic performance of MoS$_2$ monolayer for oxygen reduction reaction (ORR) by N- and P-Doping. *Electrochim. Acta.* **225**, 543–550 (2017).
35. Li, R. C. *et al.* Nitrogen doped MoS$_2$ nanosheets synthesized via a low temperature process as electrocatalysts with enhanced activity for hydrogen evolution reaction. *J. Power. Sources.* **356**, 133–139 (2017).
36. Huang, H. *et al.* High-quality phosphorus-doped MoS$_2$ ultrathin nanosheets with amenable ORR catalytic activity. *Chem. Commun.* **51**, 7903 (2015).
37. Perdew, J. P., Burke & Ernzerhof, K. M. Generalized gradient approximation made simple. *Phys. Rev. Lett.* **77**, 3865–3868 (1996).
38. Hamann, D. R., Schluter, M. & Chiang, C. Norm-conserving pseudopotentials. *Phys. Rev. Lett.* **43**, 1494–1497 (1979).
39. Dolui, K. *et al.* Possible doping strategies for MoS$_2$ monolayers: An ab initiostudy. *Phys. Rev. B* **88**, 075420 (2013).
40. Zhao, X. *et al.* Effective n-type F-doped MoSe$_2$ monolayers. *Rsc. Adv.* **7**, 26673 (2017).
41. Wang, S. *et al.* Structure and photocatalytic property of Mo-doped TiO$_2$ nanoparticles. *Powder. Technol.* **244**, 9–15 (2013).
42. Maytal, C. T. *et al.* First principles scheme to evaluate band edge positions in potential transition metal oxide photocatalysts and photoelectrodes. *Phys. Chem. Chem. Phys.* **13**, 16644–16654 (2011).
43. Yu, J. G. *et al.* New insight into the enhanced visible-light photocatalytic activities of B-, C- and B/C-doped anatase TiO$_2$ by first-principles. *Phys. Chem. Chem. Phys.* **15**, 12040 (2013).
44. Yu, J. G. *et al.* Ionic liquid assisted synthesis of uniform fluorinated B/C-Codoped TiO$_2$ nanocrystals and their enhanced visible-light photocatalytic activity. *Chem. -Eur. J* **19**, 2433–2441 (2013).

Acknowledgements

Author Contributions

The idea was proposed by Y.F.Z. and L.H. The simulations and data analyses were performed by Y.F.Z., Y.F.Z. wrote the manuscript, C.L. and W.W. prepared the table and the figures. All authors discussed the results and reviewed the manuscript.

Additional Information

Supplementary information accompanies this paper at https://doi.org/10.1038/s41598-017-17423-w.

Competing Interests: The authors declare that they have no competing interests.

Publisher's note: Springer Nature remains neutral with regard to jurisdictional claims in published maps and institutional affiliations.